Biol. Cybern. 84, 463–474 (2001)

Biological Cybernetics

Partial directed coherence: a new concept in neural structure determination

Luiz A. Baccalá[1], **Koichi Sameshima**[2]

[1] Telecommunications and Control Engineering, Escola Politécnica, University of São Paulo, Av. Prof. Luciano Gualberto, Trav. 3, 158, CEP 05508-900, Brazil
[2] Discipline of Medical Informatics & Functional Neurosurgery Laboratory, School of Medicine, University of São Paulo, Brazil

Received: 25 April 2000 / Accepted in revised form: 13 November 2000

Abstract. This paper introduces a new frequency-domain approach to describe the relationships (direction of information flow) between multivariate time series based on the decomposition of multivariate partial coherences computed from multivariate autoregressive models. We discuss its application and compare its performance to other approaches to the problem of determining neural structure relations from the simultaneous measurement of neural electrophysiological signals. The new concept is shown to reflect a frequency-domain representation of the concept of Granger causality.

1 Introduction

For many years the monitoring multiple electric signals derived from neuronal depolarization has been used to infer functional aspects of both normal and pathological brain processes. Among numerous techniques for displaying and analyzing neural signals of various types (electroencephalograms, local field potentials, and multi and single neural unit activity), methods based on the estimation of correlation/coherence functions between the activity of pairs of simultaneously analyzed structures have been the most popular approaches. These include investigating issues of physiological interest such as the determination of the source of neural activity in epileptic seizures (Duckrow and Spencer 1992) and in physiological oscillations, e.g., the alpha and theta rhythms (Lopes da Silva et al. 1973; Kocsis et al. 1994), and the activation of brain centers related to specific behavioral tasks or cognitive processes (Toyama et al. 1981; Melssen and Epping 1987; Eggermont 1990; Bressler et al. 1993; Pawelzik 1994), or the studies of the correlation between EEG waveforms and brain behavioral state, as characterized by specific patterns like typical signal amplitude and frequency as, for example, in staging the sleep state (Barlow 1979).

This state of affairs has remained largely unchanged despite the practical and theoretical limitations of coherence analysis, which merely describes instances when pairs of structures are in synchronous activity.

In fact little attention has been given to the evolution of the concept of coherence: the idea of *directed coherence* (DC) between pairs of structures. Directed coherence, rather than merely describing mutual synchronicity, tells us whether and how two structures under study are functionally connected. While ordinary coherence focuses on the structures themselves and the mutual synchrony of their activity, DC stresses their relative structural relationships by decomposing their interactions into "*feedforward*" and "*feedback*" aspects. This shift is specially relevant as even today much of the actual structural and functional connectivity in the brain is still derived from the post mortem anatomical study of experimental animals, which is unrevealing as to whether links between structures are "active" in a given scenario of brain processing that underlies the generation of some specific behavior.

In this paper (Sect. 2), we review the notion of DC as generalized to the simultaneous analysis of more than just pairs of neural structures, and place it in the perspective of the more fundamental concept of Granger causality (Granger 1969) in Sect. 3, where we further introduce a new approach of structural analysis in the frequency domain that we name *partial directed coherence* (PDC). In the examples (Sect. 4), we contrast PDC with DC to show how PDC provides direct structural information for multivariate autoregressive (MAR) models that simultaneously model many time series. PDC is used next to reveal a reversal in the direction of information flow between the cortex and the hippocampus during a spindle episode within a record of slow-wave sleep.

Correspondence to: L. A. Baccalá
(e-mail: baccala@lcs.poli.usp.br)

2 Background: generalization of directed coherence

Descriptions of the interaction between areas of the brain have relied on estimates of the cross-spectral density matrix

$$\mathbf{S}(f) = \begin{bmatrix} S_{11}(f) & S_{12}(f) & \cdots & S_{1N}(f) \\ S_{21}(f) & S_{22}(f) & \cdots & S_{2N}(f) \\ \vdots & \vdots & \ddots & \vdots \\ S_{N1}(f) & S_{N2}(f) & \cdots & S_{NN}(f) \end{bmatrix} \tag{1}$$

of the measured signals $\mathbf{x_i}(n), 1 \leq i \leq N$.

When analyzing two series at a time, the most widely used and classically accepted frequency-domain method studies the *ordinary coherence* functions

$$C_{ij}(f) = \frac{|S_{ij}(f)|^2}{S_{ii}(f)S_{jj}(f)} \tag{2}$$

that express the simultaneous activation (degree of relative synchrony) between areas i and j under scrutiny (Bendat and Piersol 1986). For frequencies where $C_{ij}(f)$ is high, one can adequately model the observed interaction through a linear operator T_{ji}, i.e.,

$$X_j(f) = T_{ji}X_i(f) \ , \tag{3}$$

where also one may alternatively employ the inverse operator of $T_{ij} = T_{ji}^{-1}$ which produces an equally suitable alternative description to (3) in the form

$$X_i(f) = T_{ij}X_j(f) = T_{ji}^{-1}X_j(f) \ . \tag{4}$$

This freedom of choice between either (3) or (4) leads to an ambiguity of description, with one being no more appropriate than the other.

To resolve this dilemma of arbitrary descriptive choice, Saito and Harashima (1981) used information theoretic arguments to introduce the notion of DC which amounts to a *unique* decomposition of the ordinary coherence function $C_{ij}(f)$ into two "directed coherences": one representing the *feedforward* and the other representing the *feedback* aspects of the interaction between the structures under study. In the original proposal, bivariate autoregressive time-series modelling was used to compute the directed coherences from the factorization of (1) when $N = 2$. A practical use of the DC was reported by Schnider et al. (1989) in a study of Parkinson's tremor.

Some attempts of generalization of directed coherence to more than two simultaneously analyzed time series followed (Kaminski and Blinowska 1991; Baccalá and Sameshima 1998; Baccalá et al. 1998). Much as for $N = 2$, these generalizations rest on a general spectral factorization result (Gevers and Anderson 1981, 1982) whereby the cross-spectral power density matrix $\mathbf{S}(f)$ can be factored as

$$\mathbf{S}(f) = \mathbf{H}(f)\Sigma\mathbf{H}^{\mathrm{H}}(f) \tag{5}$$

where the superscript H stands for Hermitian transpose and

$$\mathbf{H}(f) = \begin{bmatrix} H_{11}(f) & H_{12}(f) & \cdots & H_{1N}(f) \\ H_{21}(f) & H_{22}(f) & \cdots & H_{2N}(f) \\ \vdots & \vdots & \ddots & \vdots \\ H_{N1}(f) & H_{N2}(f) & \cdots & H_{NN}(f) \end{bmatrix}$$

$$= [\,\mathbf{h}_1(f) \quad \mathbf{h}_2(f) \quad \cdots \quad \mathbf{h}_N(f)\,]$$

is a matrix of suitable filters described in the frequency domain and where

$$\Sigma = \begin{bmatrix} \sigma_{11}^2 & \sigma_{12} & \cdots & \sigma_{1N} \\ \sigma_{21} & \sigma_{22}^2 & \cdots & \vdots \\ \vdots & \vdots & \ddots & \vdots \\ \sigma_{N1} & \cdots & \cdots & \sigma_{NN}^2 \end{bmatrix}$$

is a covariance matrix. Use the factors in (5) lead to the following immediate generalized definition of the DC from j to i as (Baccalá and Sameshima 1998; Baccalá et al. 1998):

$$\gamma_{ij}(f) = \frac{\sigma_{jj}H_{ij}(f)}{\sqrt{S_{ii}(f)}} \ , \tag{6}$$

where

$$S_{ii}(f) = \sum_{j=1}^{N} \sigma_{jj}^2 |H_{ij}(f)|^2 \ , \tag{7}$$

which reduces to Saito and Harashima's (1981) definition when $N = 2$.

One additional important restriction of the original Saito–Harashima method is their explicit presumption that Σ is diagonal ($\sigma_{ij} = 0$ for $i \neq j$). In that case $|\gamma_{ij}(f)^2|$ can be interpreted as the fraction of the power contributing to the total power in $x_i(n)$ that originates in $x_j(n)$ at frequency f.

For diagonal Σ one can show that the ordinary coherence can be written as

$$C_{ij}(f) = \gamma_i^{\mathrm{H}}(f)\gamma_j(f) = \sum_{k=1}^{N} \gamma_{ik}^*(f)\gamma_{kj}(f) \tag{8}$$

where $\gamma_i(f) \stackrel{\Delta}{=} [\gamma_{i1}(f), \ldots, \gamma_{iN}(f)]^{\mathrm{T}}$ with * standing for the complex conjugate. This justifies the name DC as $\gamma_{ij}(f)$ can be interpreted as a measure of the influence from $x_j(n)$ onto $x_i(n)$ as opposed to $\gamma_{ji}(f)$ which describes the contribution in the opposite direction.

Remark 1. It is easy to show that redefining DC as

$$\bar{\gamma}_{ij}(f) = \frac{H_{ij}(f)}{\sqrt{S_{ii}(f)}} \tag{9}$$

allows writing the ordinary coherence in full generality as

$$C_{ij}(f) = \bar{\gamma}_{\mathrm{i}}{}^{\mathrm{H}}(f)\Sigma\bar{\gamma}_i(f) \ , \tag{10}$$

with $\bar{\gamma}_i(f) \triangleq [\bar{\gamma}_{i1}(f), \ldots, \bar{\gamma}_{iN}(f)]^{\mathrm{T}}$, where

$S_{ii}(f) = \mathbf{h}_i^{\mathrm{H}}(f)\Sigma\mathbf{h}_i(f)$,

even if Σ is not diagonal.

Because of the restriction of Saito and Harashima (1981) to diagonal Σ, Kaminski and Blinowska (1991) introduced an alternative quantity to describe interactions among neural elements that forsakes Σ altogether. They termed their estimator the "*directed transfer function*" (DTF). It coincides with the magnitude of (6) when σ_{jj} are all set to 1, i.e.,

$$DTF_{ij}(f) = \frac{H_{ij}(f)}{\sqrt{\sum_{j=1}^{N} |H_{ij}(f)|^2}} = \frac{H_{ij}(f)}{\sqrt{\mathbf{h}_i^{\mathrm{H}}(f)\mathbf{h}_i(f)}} \quad . \tag{11}$$

In practice, DC/DTF estimation makes extensive use of multichannel autoregressive models of the form (Franaszczuk et al. 1985; Schnider et al. 1989; Kaminski and Blinowska 1991; Franaszczuk et al. 1994; Kaminski et al. 1997; Korzeniewska et al. 1997; Baccalá and Sameshima 1998; Baccalá et al. 1998):

$$\begin{bmatrix} x_1(n) \\ \vdots \\ x_N(n) \end{bmatrix} = \sum_{r=1}^{p} \mathbf{A}_r \begin{bmatrix} x_1(n-r) \\ \vdots \\ x_N(n-r) \end{bmatrix} + \begin{bmatrix} w_1(n) \\ \vdots \\ w_N(n) \end{bmatrix} \tag{12}$$

wherefrom the joint spectral density estimate of (5) is obtained by

$$\mathbf{H}(f) = \bar{\mathbf{A}}^{-1}(f) = (\mathbf{I} - \mathbf{A}(f))^{-1} \tag{13}$$

and where Σ is the covariance matrix of $w_i(n)$, while

$$\mathbf{A}(f) = \sum_{r=1}^{p} \mathbf{A}_r z^{-r}\Big|_{z=\mathrm{e}^{-\mathrm{i}2\pi f}} \text{with}$$

$$\mathbf{A}_r = \begin{bmatrix} a_{11}(r) & a_{12}(r) & \cdots & \cdots & a_{1N}(r) \\ \vdots & \vdots & \vdots & \vdots & \vdots \\ \vdots & \vdots & \vdots & a_{ij}(r) & \vdots \\ \vdots & \vdots & \vdots & \vdots & \vdots \\ a_{N1}(r) & \cdots & \cdots & \cdots & a_{NN}(r) \end{bmatrix}$$

where the coefficients $a_{ij}(r)$ represent the linear interaction effect of $x_j(n-r)$ onto $x_i(n)$.

3 Granger causality and the new approach

In their original paper, Saito and Harashima (1981) refer to a possible rationale for their method in what is now known as Granger causality (Granger 1969). By definition, *an observed time series $x_j(n)$ Granger-causes another series $x_i(n)$, if knowledge of $x_j(n)$'s past significantly improves prediction of $x_i(n)$*; this kind of predictability improvement is not reciprocal, i.e., $x_j(n)$ may Granger-cause $x_i(n)$ without $x_i(n)$ necessarily Granger-causing $x_j(n)$.

Conceptually, Granger causality is a well-defined idea originating in econometrics where it possesses several statistical testing procedures (Lutkepöhl 1993). Its key notion is the *exclusive* consideration of past samples in prediction improvements. When the present sample of $x(n)$ contributes significantly to the predictions of $y(n)$, it is usual to speak of *instantaneous Granger causality*. It is important to keep in mind that these forms of causality are distinct: the first refers to exclusive use of the past of a time series in helping predict another time series, while instantaneous Granger causality concerns itself only with the predictability effect of the present of one time series upon another time series. Most important for now is that statistical tests of lack of instantaneous Granger causality reduce to showing that Σ is diagonal.

Assessing the extent of Granger causality provides a measure of the strength of interaction between structures under the rationale that predictable variations in a series – due to the consistent emergence of variations in another series – takes place if their mechanisms of generation are somehow physically linked, as with active neuroanatomic connections.

Some statistical Granger causality tests (GCTs) are based on the direct examination of the $a_{ij}(r)$ coefficients in MAR modelling, as the latter describe the linear prediction effect of the rth past sample $x_j(n-r)$ of $x_j(n)$ on predicting $x_i(n)$. Thus, if one may statistically show that $a_{ij}(r) = 0$ for all values of r, the hypothesis of $x_j(n)$ Granger-causing $x_i(n)$ can be rejected. A specific conventional test of this kind applicable to the joint process of multiple neural signals is reviewed in Baccalá and Sameshima (1998). Other tests are contained in Lutkepöhl (1993).

The main drawback of most Granger causality tests, is that, unlike what happens for DC, a frequency-domain picture of the interaction between neural structures is usually unavailable except when $N = 2$ (Geweke 1982).

Furthermore, to gauge relationships between pairs of time series when processing $N > 2$, one often observes conflicting results between DC/DTF and Granger causality tests, i.e., $x_i(n)$ may have high DC to $x_j(n)$ and yet it may be possible to reject Granger causality from $x_i(n)$ to $x_j(n)$ using conventional GCT. As a matter of fact, this happens frequently when simultaneously analyzing more than two time series. By contrast, when $N = 2$ (Example 1), DC/DTF and Granger causality tests always agree.

To provide a frequency-domain picture for Granger causality descriptions, we propose the novel concept of PDC. It is based on another popular quantifier of the relationship between pairs of signals – the so-called *partial coherence function*, $|\kappa_{ij}(f)|^2$, that describes the interaction between $x_i(n)$ and $x_j(n)$ when the influence due to all other $N-2$ time series is discounted. The key result is the following factorization (Baccala, personal communication, 2000):

$$\kappa_{ij}(f) = \frac{\bar{\mathbf{a}}_i^{\mathrm{H}}(f)\Sigma^{-1}\bar{\mathbf{a}}_j(f)}{\sqrt{(\bar{\mathbf{a}}_i^{\mathrm{H}}(f)\Sigma^{-1}\bar{\mathbf{a}}_i(f))(\bar{\mathbf{a}}_j^{\mathrm{H}}(f)\Sigma^{-1}\bar{\mathbf{a}}_j(f))}} \quad , \tag{14}$$

where Σ is the prediction error covariance matrix associated with the model in (12), and $\bar{\mathbf{a}}_k(f)$ is the kth column of the matrix

$$\bar{\mathbf{A}}(f) = \mathbf{I} - \mathbf{A}(f) = [\bar{\mathbf{a}}_1(f)\bar{\mathbf{a}}_2(f)\ldots\bar{\mathbf{a}}_N(f)] \ .$$

By analogy with (10) – where the DC reflects terms into which one can decompose the ordinary coherence – we may adopt the following general definition:

Definition 1. The *partial directed coherence factor* (PDCF) from j to i is given by

$$\pi_{ij}(f) \triangleq \frac{\bar{A}_{ij}(f)}{\sqrt{\bar{\mathbf{a}}_j^{\mathrm{H}}(f)\sum^{-1}\bar{\mathbf{a}}_j(f)}} \tag{15}$$

where $\bar{A}_{ij}(f)$ is the i, jth element of $\bar{\mathbf{A}}(f)$.

It follows immediately that the partial coherence between i and j is given by

$$\kappa_{ij}(f) = \pi_i^{\mathrm{H}}(f)\Sigma^{-1}\pi_j(f) \tag{16}$$

for $\pi_i(f) \triangleq [\pi_{1i}(f),\ldots,\pi_{Ni}(f)]^{\mathrm{T}}$, whence the motivation for $\pi_{ij}(f)$'s name.

Because

$$\bar{A}_{ij}(f) = \begin{cases} 1 - \sum_{r=1}^{p} a_{ij}(r)\mathrm{e}^{-i2\pi fr}, & \text{if } i = j \\ -\sum_{r=1}^{p} a_{ij}(r)\mathrm{e}^{-i2\pi fr}, & \text{otherwise} \end{cases} \tag{17}$$

the PDCF depends mostly on the $a_{ij}(r)$ coefficients that describe the relationships between the present of time series $x_i(n)$ and the past of $x_j(n)$ as compared to $x_j(n)$'s past effect on the other time series.

Because Σ affects the denominator, (16) mixes Granger causality with instantaneous Granger causality. To completely remove the instantaneous effects, one might prefer to describe Granger causality relations alone through

$$\bar{\pi}_{ij}(f) \triangleq \frac{\bar{A}_{ij}(f)}{\sqrt{\bar{\mathbf{a}}_j^{\mathrm{H}}(f)\bar{\mathbf{a}}_j(f)}} \tag{18}$$

which is a function of $a_{ij}(r)$ alone, forsaking Σ in a completely analogous fashion to DTF. Obviously a diagonal Σ with equal unit variances in (15) simplifies to (18).

Hence to portray Granger causality exclusively as opposed to its mixture with instantaneous Granger causality, we adopt:

Definition 2. The *partial directed coherence* (PDC) from j to i is given by (18).

Note also that, as for DC/DTF (Baccalá and Sameshima 1998) the following normalization properties hold:

$$0 \le |\bar{\pi}_{ij}(f)|^2 \le 1 \tag{19}$$

and

$$\sum_{i=1}^{N} |\bar{\pi}_{ij}(f)|^2 = 1 \ , \tag{20}$$

for all $1 \le j \le N$.

Because of the latter normalization conditions, $\bar{\pi}_{ij}(f)$ represents the relative coupling strength of the interaction of a given signal source structure j with regard to structure i as compared to all of j's interactions to other structures. As such, PDC ranks the relative interaction strengths with respect to a given signal source.

Remark 2. This is an important difference between DC/DTF and PDCF/PDC since $\gamma_{ij}(f)$ is normalized with respect to the structure that receives the signal, whereas $\pi_{ij}(f)$ is normalized with respect to the structure that sends the signal.

Remark 3. It turns out the equality in (20) is only a special case of normalization that could equally be applied to PDCF. If we define the square of the vector norm of the vector $\pi_j(f)$ as $|\pi_j(f)|^2 = \pi_j^{\mathrm{H}}(f)\Sigma^{-1}\pi_j(f)$, the general result is $|\pi_j(f)|^2 = 1$.

Remark 4. When $i = j$, the PDC $|\bar{\pi}_{ii}(f)|$ functions describe the fraction of the time evolution represented by exclusive consideration of $x_i(n)$'s own past on itself that is not explicable by the other measured time series; in other words, it represents how much its own past couples to its present state, whereas the $|DTF_{ii}(f)|$ reflect the power density due to none of the other series.

3.1 Additional comments

3.1.1 Instantaneous granger causality. In the linear least-mean-squared error prediction context, one can show that Σ is diagonal if the present state of a series adds little to the prediction of other time series (Lutkepöhl 1993). Relationships between present samples of the $x_i(n)$ time series are described exclusively by correlations among the $w_i(n)$ processes. Several tests exist to check for the diagonality of Σ (Lutkepöhl 1993).

Suppressing the use of Σ as in (18) (or in Eq. 11, as $H(f)$ is actually computed exclusively from $A(f)$) is what specializes the problem to the exclusive consideration of past values in prediction. This is precisely in tune with the Granger causality picture and contrasts with the multivariate Granger causality test reviewed in Lutkepöhl (1993) and Baccalá et al. (1998) which is, at least in part, affected by the full structure of Σ exactly as happens for PDCF inference using (15).

3.1.2 Computational advantages of PDC. Because PDC makes direct use of $\mathbf{A}(f)$ in (12), it has the advantage of dispensing with the matrix inversion in (13) for each frequency of interest. This is computationally more efficient and avoids numerical imprecisions that might

result from possible ill-conditioning of $\bar{\mathbf{A}}(f)$ at some frequencies. This can be critically important in view of the use of small data samples in practical estimation.

3.1.3 Variations on PDC estimate. As in the definition of DC (6), one possible variation in PDC estimation can take into account large amplitude differences in the $x_i(n)$ signals by using just the diagonal elements of Σ^{-1} as weighting factors of each component in $\bar{\mathbf{a}}_i(f)$.

Alternative means of normalization for $\bar{A}_{ij}$ are possible and are under study. None of them, however, can be interpreted as immediately related to partial coherence.

4 Illustrative Examples

Previously published methods using DC and close variants restrict themselves either to diagonal Σ or by forsaking the Σ structure, so in this paper we employ only PDC (18) in the following examples. We begin with a theoretical example showing PDC's equivalence to DTF when $N = 2$.

Example 1. When only two series, $N = 2$, are being analyzed simultaneously, the interaction analysis can be approached using either (6) or (15). This is possible because $H_{ij}(f)$ is proportional to $\bar{\mathbf{A}}_{ij}(f)$ $(i \neq j)$, where nullity of one implies nullity of the other, indicating lack of influence in $x_i(n)$ that is attributable to $x_j(n)$. In fact, the resulting $|DTF_{ij}(f)|$ and $|\bar{\pi}_{ij}(f)|$ are equal for $i \neq j$. It is easy to see this from (6) as

$$|DTF_{ij}(f)| = \frac{|H_{ij}(f)|}{\sqrt{|H_{i1}(f)|^2 + |H_{i2}(f)|^2}}$$

and

$$\bar{\mathbf{A}}(f) = \begin{bmatrix} \bar{A}_{11}(f) & \bar{A}_{12}(f) \\ \bar{A}_{21}(f) & \bar{A}_{22}(f) \end{bmatrix} = \begin{bmatrix} H_{11}(f) & H_{12}(f) \\ H_{21}(f) & H_{22}(f) \end{bmatrix} = \frac{1}{\Delta} \begin{bmatrix} H_{22}(f) & -H_{12}(f) \\ -H_{21}(f) & H_{11}(f) \end{bmatrix},$$

with $\Delta = H_{11}(f)H_{22}(f) - H_{12}(f)H_{21}(f)$, so that

$$|\bar{\pi}_{ij}(f)| = \frac{|\bar{A}_{ij}(f)|}{\sqrt{|\bar{A}_{1j}(f)|^2 + |\bar{A}_{2j}(f)|^2}} \tag{21}$$

leads upon substitution to

$$|\bar{\pi}_{12}(f)| = \frac{|-H_{12}(f)|}{\sqrt{|-H_{12}(f)|^2 + |H_{22}(f)|^2}} = |\gamma_{12}(f)|$$

and

$$|\bar{\pi}_{21}(f)| = \frac{|-H_{21}(f)|}{\sqrt{|H_{22}(f)|^2 + |-H_{21}(f)|^2}} = |\gamma_{21}(f)| \ . \tag{22}$$

Note that the equalities do not occur for identical indices; i.e., we have $|\gamma_{11}(f)| = |\bar{\pi}_{22}(f)|$ and $|\gamma_{22}(f)| = |\bar{\pi}_{11}(f)|$.

In the following examples we compute DTF and PDC for known models to show that the estimators produce different results for $N > 2$ simultaneously modelled series.

Example 2. Suppose that three simultaneously observed time series were generated by the equations:

$$\begin{cases} x_1(n) = 0.5x_1(n-1) + 0.3x_2(n-1) + 0.4x_3(n-1) \\ \qquad\quad + w_1(n) \\ x_2(n) = -0.5x_1(n-1) + 0.3x_2(n-1) + 1.0x_3(n-1) \\ \qquad\quad + w_2(n) \\ x_3(n) = -0.3x_2(n-1) - 0.2x_3(n-1) + w_3(n) \end{cases} \tag{23}$$

where $w_i(n)$ are zero-mean uncorrelated white processes with identical variances. One readily sees that only $x_3(n)$ is not influenced explicitly by the past state of $x_1(n)$.

The corresponding $|DTF_{ij}(f)|$ and $|\bar{\pi}_{ij}(f)|$ are plotted in a matrix layout in Fig. 1, and show that an explicit

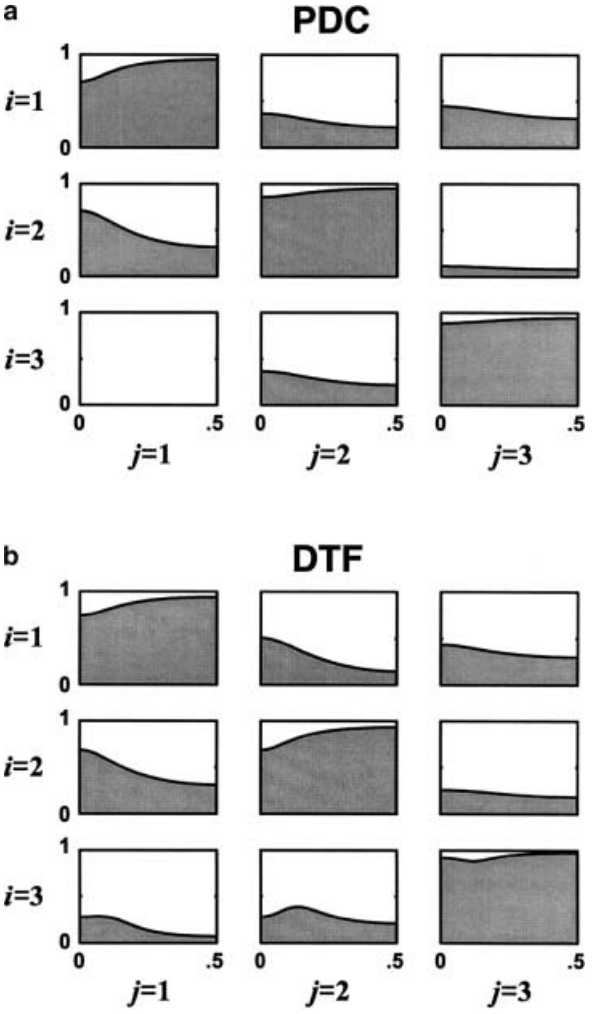

Fig. 1. a Matrix layout plots for partial directed coherence PDC, $|\bar{\pi}_{ij}(f)|$, and **b** $|DTF_{ij}(f)|$ describing (23). Of note is that $\bar{\pi}_{31}(f) = 0$ reflects the immediate independence of $x_3(n)$ on $x_1(n)$. This same information cannot be obtained by inspecting $DTF_{31}(f)$. See Remark 4 for the meaning of plots when $i = j$

direct lack of influence is only fully described by the latter where $|\pi_{31}(f)| = 0$, as opposed to what happens to $|DTF_{31}(f)|$.

Uses of DTF have centered around the determination of perturbation foci (Franaszczuk et al. 1994; Kaminski et al. 1997), so consider:

Example 3. In the interconnection structure summarized in Fig. 2a, the signal propagates from a measured driving oscillating source $x_1(n)$ to $x_2(n)$ and independently to $x_3(n)$. The signal $x_1(n)$ also couples to what would be an otherwise independent oscillator comprised of $x_4(n)$ and $x_5(n)$ if there were no coupling from $x_1(n)$. Employing a specific matching MAR model (see caption of Fig. 2), results in $|\bar{\pi}_{ij}(f)| = 0$ (Fig. 2b) whenever no direct connection exists in Fig. 2a, whereas $|DTF_{ij}(f)| \neq 0$ (Fig. 2c) for all j when $i = 1$, and also for $DTF_{45}(f)$ and $DTF_{54}(f)$. Thus the structural mapping of the series is not clearly represented in a direct way in Fig. 2c.

Example 4. In Fig. 3a, the signal from a measured oscillating driving source $x_1(n)$ propagated sequentially to $x_2(n)$ and $x_3(n)$ (noise corrupted and attenuated forms of $x_1(n)$), which couples into an otherwise independent oscillator comprised of $x_4(n)$ and $x_5(n)$. Again employing a specific matching MAR model (see caption of Fig. 3) results in $|\bar{\pi}_{ij}(f)| = 0$ (Fig. 3b) whenever there is no direct connection in Fig. 3a; i.e., no explicit dependence of $x_i(n)$ on the past states of the other series, whereas in Fig. 3c, $|DTF_{ij}(f)| \neq 0$ for all $i \geq j$ and also for $|DTF_{45}(f)|$, leading to the conclusion that the structural mapping is not as clearly apparent through $DTF_{ij}(f)$ as for $\bar{\pi}_{ij}(f)$.

Example 5. Closing the loop from $x_5(n)$ into $x_1(n)$ of the previous example results in Fig. 4a with a specific matching MAR model described in the caption of Fig. 4. This reveals that plotting $|\bar{\pi}_{ij}(f)|$ (Fig. 4b) still reflects the underlying structure, whereas little inference can be made from $DTF_{ij}(f)$ which is nonzero for all i and j (Fig. 4c).
Finally consider:

Example 6. A structural change in Fig. 3a, which yields Fig. 5a, whose $DTF_{ij}(f)$ (Fig. 5c) is virtually identical to that of Fig. 3c, but its structural differences are easy to pinpoint through $\bar{\pi}_{ij}(f)$ (Fig. 5b).

Remark 5. In all of these examples, $DTF_{ij}(f)$ is nonzero whenever there is some signal pathway that goes from structure j to structure i in the structural graphs that describe the model. While DTF marks the existence of signal pathways connecting structures either directly or indirectly, PDC resolves the existence of direct connection between pairs of structures.

4.1 PDC analysis of synchronized sleep data

Figure 6 contains a 30-s record of slow-wave sleep in the rat with a spindle episode between 13 and 15 s as

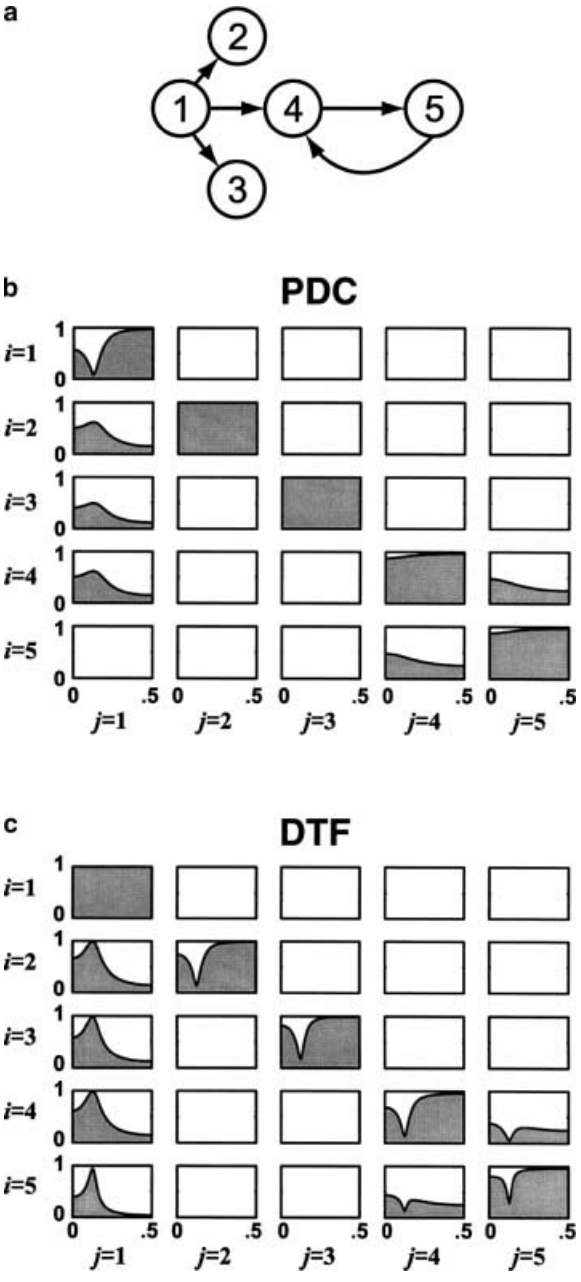

Fig. 2. **a** Diagram depicting the mutual influences on each series due to the past states of the other series, corresponding to the multivariate autoregressive model given by

$$\begin{cases} x_1(n) = 0.95\sqrt{2}x_1(n-1) - 0.9025x_1(n-2) + w_1(n) \\ x_2(n) = 0.5x_1(n-2) + w_2(n) \\ x_3(n) = -0.4x_1(n-3) + w_3(n) \\ x_4(n) = -0.5x_1(n-2) + 0.25\sqrt{2}x_4(n-1) \\ \qquad +0.25\sqrt{2}x_5(n-1) + w_4(n) \\ x_5(n) = -0.25\sqrt{2}x_4(n-1) + 0.25\sqrt{2}x_5(n-1) + w_5(n) \end{cases}$$

In comparing the equations to the diagram one readily sees $x_1(n)$ as a direct source to $x_2(n)$, $x_3(n)$, and $x_4(n)$. If isolated, $x_4(n)$ and $x_5(n)$ would themselves alone form an oscillator. There is no direct coupling from $x_1(n)$ to $x_5(n)$. Each variable in the model is affected by additive noise (not displayed in **a**). The corresponding $|\bar{\pi}_{ij}(f)|$ and $|DTF_{ij}(f)|$ are plotted in **b** and **c**. Note the immediate mapping of $|\bar{\pi}_{ij}(f)| = 0$ whenever direct connection is lacking. Except for $|DTF_{51}(f)| \neq 0$, the same lack of nullity in $|DTF_{ij}(f)|$ points to the same structural inference as $|\bar{\pi}_{ij}(f)|$. See Remark 4 for the meaning of plots when $i = j$

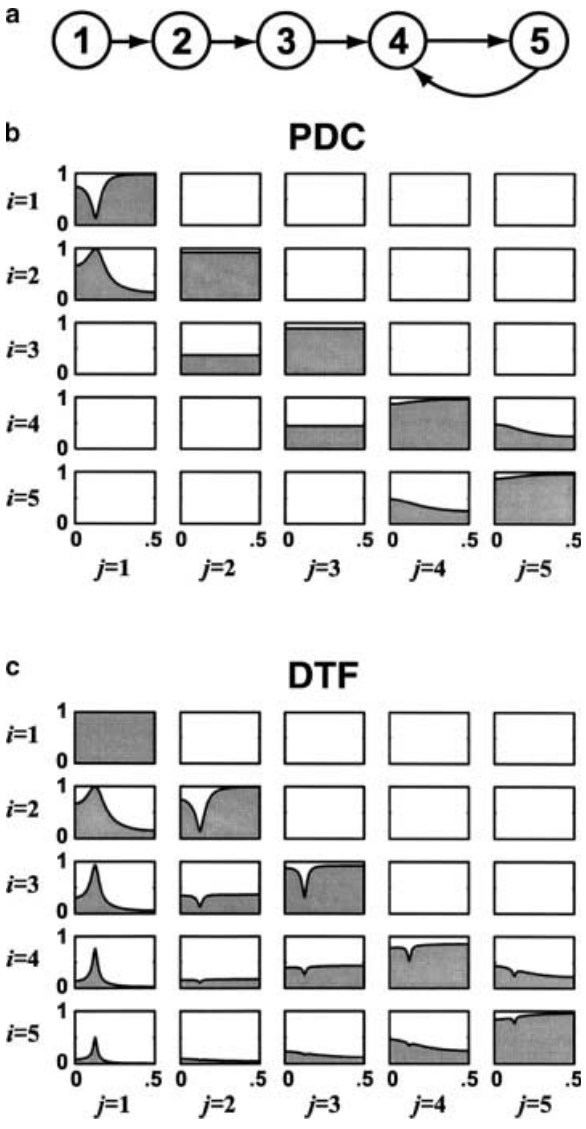

Fig. 3. **a** Diagram modified from that of Fig. 2a when now $x_1(n)$ directly influences $x_2(n)$ only, which in turn modifies $x_3(n)$, and then finally couples to $x_4(n)$. As before, $x_4(n)$ and $x_5(n)$ would form an oscillator if isolated. Dynamically the signal propagation situation can be formalized as

$$\begin{cases} x_1(n) = 0.95\sqrt{2}x_1(n-1) - 0.9025x_1(n-2) + w_1(n) \\ x_2(n) = -0.5x_1(n-1) + w_2(n) \\ x_3(n) = 0.4x_2(n-2) + w_3(n) \\ x_4(n) = -0.5x_3(n-1) + 0.25\sqrt{2}x_4(n-1) \\ \qquad +0.25\sqrt{2}x_5(n-1) + w_4(n) \\ x_5(n) = -0.25\sqrt{2}x_4(n-1) + 0.25\sqrt{2}x_5(n-1) + w_5(n) \end{cases}$$

As before, **b** and **c** contain $|\bar{\pi}_{ij}(f)|$ and $|DTF_{ij}(F)|$, respectively. Again, immediate mapping only of $|\bar{\pi}_{ij}(f)| = 0$ shows lack of a direct connection. The pattern of $|DTF_{ij}(f)| \neq 0$ spans the lower diagonals of the matrix. See Remark 4 for the meaning of plots when $i = j$

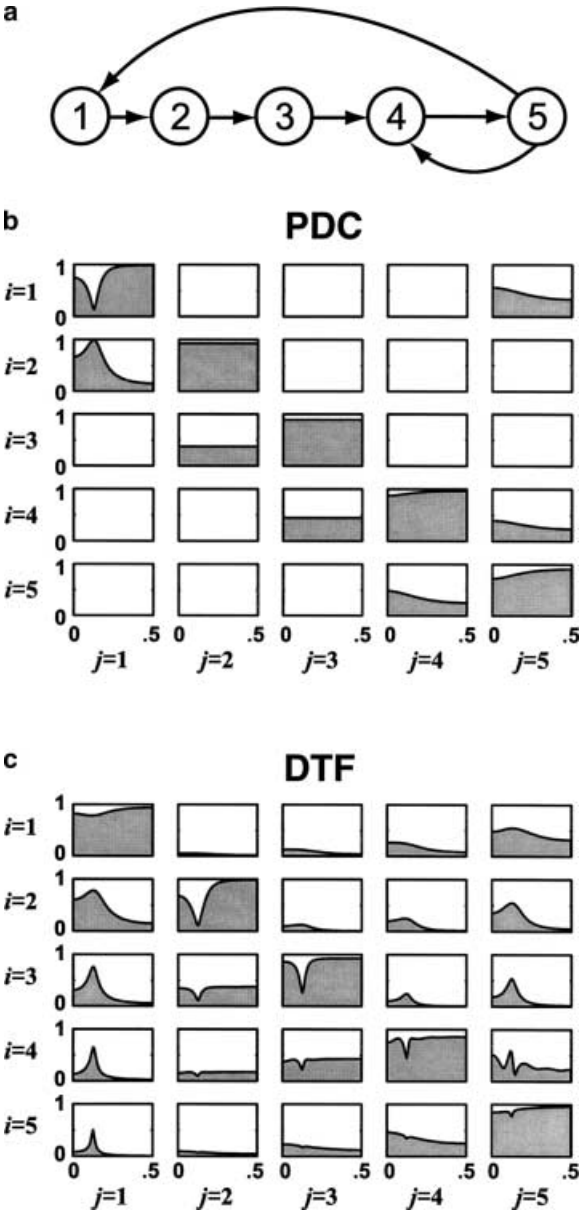

Fig. 4. **a** In this example the loop is closed from $x_5(n)$ back to $x_1(n)$ via a direct connection; i.e., now the first equation in the caption of Fig. 3 becomes:

$$x_1(n) = 0.95\sqrt{2}x_1(n-1) - 0.9025x_1(n-2) + 0.5x_5(n-2) + \omega_1(n) \ .$$

b As before, the mappings of direct coupling are preserved by $|\bar{\pi}_{ij}(f)|$. **c** Whereas $|DTF_{ij}(f)| \neq 0$ for all values. This gives no hint as to actual direct connections. See Remark 4 for the meaning of plots when $i = j$

monitored from cortical areas (A10, A3, and A17) and hippocampal fields (CA1 and CA3) and the dentate gyrus (DG). These six signals were simultaneously subjected to analysis using MAR modelling, wherefrom PDC estimates were computed for 2-s-long segments and 50% overlap between them. The resulting time-frequency evolution of PDC is displayed in Fig. 7 for A10 and CA1, whose interaction switches directionality during a spindle episode that starts at around second 13 and lasts roughly 2 s. Note that the interaction between these areas was preceeded by an increase in PDC from A10 to CA1 which changed direction during the episode itself. Also note the increase in ordinary coherence roughly 8 s before and after the spindle.

Combined detailed summaries of PDC and DTF respectively for the pre-spindle and spindle periods are

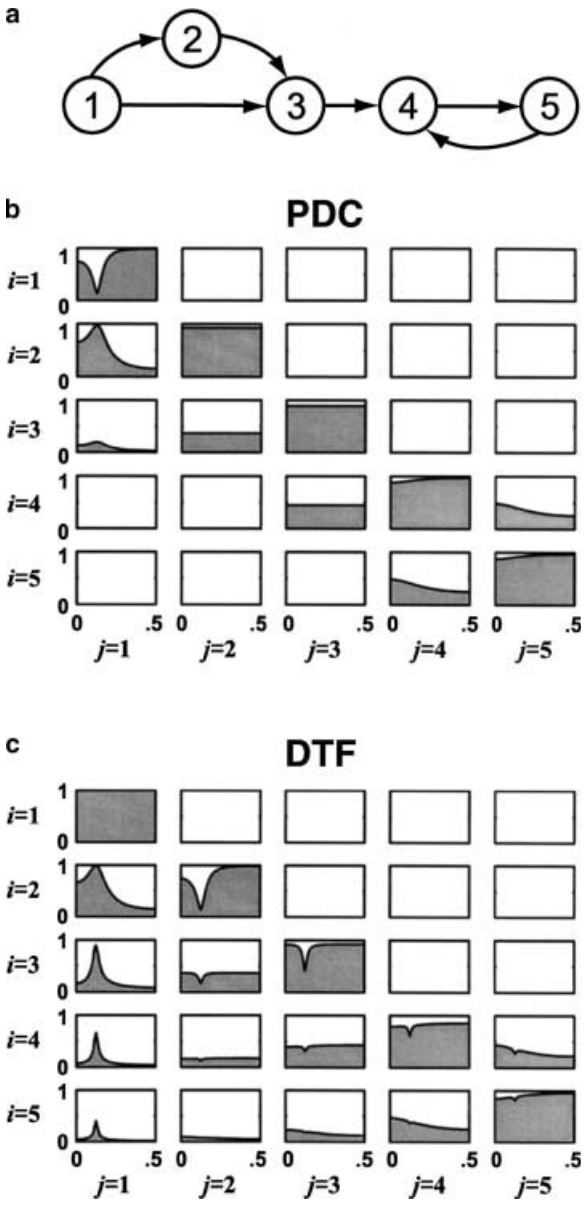

Fig. 5. a Depicts a structure modified from Fig. 3, where $x_1(n)$ connects to $x_4(n)$ via two distinct pathways, through $x_2(n)$ and $x_3(n)$, respectively. That is,

$$\begin{cases} x_1(n) = 0.95\sqrt{2}x_1(n-1) - 0.9025x_1(n-2) + w_1(n) \\ x_2(n) = -0.5x_1(n-1) + w_2(n) \\ x_3(n) = 0.1x_1(n-4) - 0.4x_2(n-2) + w_3(n) \\ x_4(n) = -0.5x_3(n-1) + 0.25\sqrt{2}x_4(n-1) \\ \qquad +0.25\sqrt{2}x_5(n-1) + w_4(n) \\ x_5(n) = -0.25\sqrt{2}x_4(n-1) + 0.25\sqrt{2}x_5(n-1) + w_5(n) \end{cases}$$

Clearly, $DTF_{ij}(f)$ (Fig. 5c vs. Fig. 3c) fail to portray the structural differences that $\bar{\pi}_{ij}(f)$ (Figs. 5b and 3b) reveal immediately. See Remark 4 for the meaning of plots when $i = j$

available in Figs. 8 and 9 for all the simultaneously analyzed structures. These figures also contain schematic structural diagrams (graphs) associated with PDC and DTF for each period. These graphs were constructed using the maximum values of PDC and DTF in Tables 1 and 2. Interaction strength was portrayed using arrow types and widths on a five-level scale similar to that used in Fig. 7 (no arrow below 0.2).

One readily sees that the pre-spindle period lacks hippocampal feedback to cortex (see PDC Fig. 8a and c). Except for links from DG to A17 and from CA3 to A17 (see Sect. 5.2 for a discussion on the unavailability of rigorous confidence levels), DTF marks of the existence of links (whether direct or indirect) between the structures involved. Note that the DTF graph (Fig. 8d) is consistent with the non-existence of a signal pathway from A10 to A3 in the PDC graph (Fig. 8c).

This contrasts sharply with the spindle episode when PDC (Figs. 9a and c) allows discriminating feedback from hippocampal structures to cortex, mostly via CA1 through A10. PDC also permits the visualization of the signal propagation pattern in the cortex from A17 (a sensory area) through A3 and A10 (motor area) that ultimately feeds back to A17. The DTF graph (Fig. 9c), on the other hand, is unable to portray these signal flow details as most structures are bidirectionally linked, confirming the existence of signal pathways (direct and indirect links) with various strengths connecting all the structures.

5 Discussion

In developing PDC we provide an alternative frequency-domain representation of multivariate processes grounded on the notion of Granger causality and which adds to the notion of DC/DTF. This is specially important because of the conflict between DTF (as in Example 2) with test designed to infer the linear causal structure (GCT) between members of multiple time series (Baccalá et al. 1998). Much of the rationale behind this proposal is that Granger causality between time series is a more fundamental notion compared to ideas like DTF when $N > 2$. As portrayed in our examples, plotting $\pi_{ij}(f)$ provides graphical representations of the structural interaction in which $\pi_{ij}(f)$ nullity follows immediately from $a_{ij}(r) = 0$ $(1 \leq r \leq p)$, indicating lack of Granger causality.

5.1 Comparison between DC/DTF and PDC

Our examples expose cases when DC/DTF and PDC (and GCT) must agree. A basic result is that they always agree for $N = 2$, as shown theoretically in Example 1. When $N > 2$, time series are analyzed simultaneously; DTF nullity implies PDC nullity and vice versa only if the structure of the $\mathbf{H}(f)$ matrix is preserved upon inversion (as for upper (lower) triangular matrices, whose inverse is also upper (lower) triangular). In cases such as this, aside from the issues of statistical and numerical reliability, DTF and PDC lead to identical conclusions as to the interaction between pairs of structures.

While $\pi_{ij}(f)$ provides explicit information about structure by expressing the direct interactions, $\gamma_{ij}(f)$ furnishes indirect information about such interaction. As discussed in Baccalá and Sameshima (1998) and Baccalá

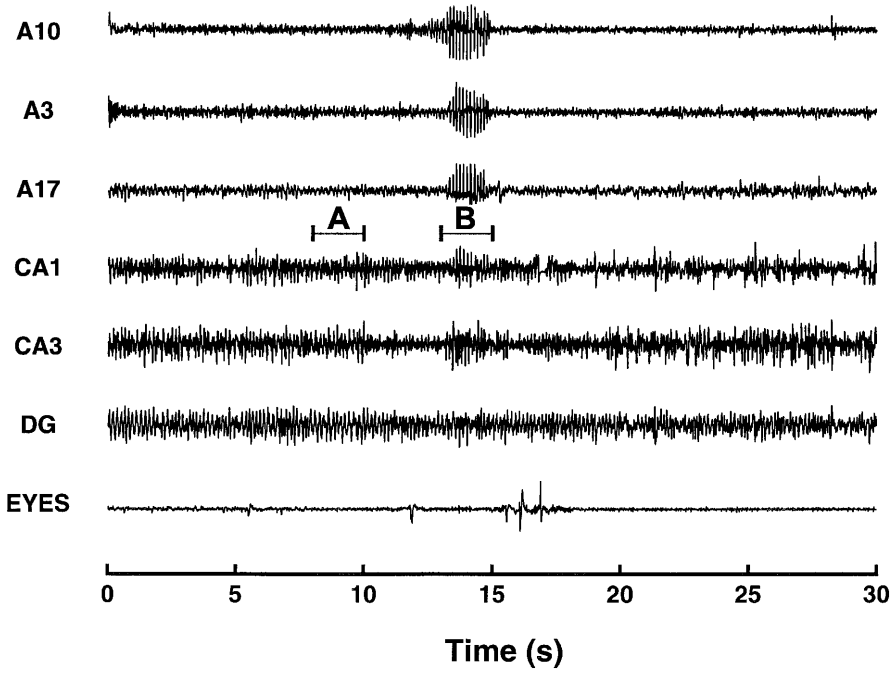

Fig. 6. A thirty-second-long local field-potential recording from rat in slow wave sleep in which a spindle episode occurred between 13 and 15 s as monitored from left hemisphere of cortical areas *A10*, *A3*, and *A17*, and hippocampal *CA1* and *CA3* fields, and the dentate gyrus (*DG*). The measurements were sampled at 256 Hz with 10-bit resolution using bipolar microelectrodes with a 1-mm tip separation. The *lower trace* (*EYES*) monitored muscle activity related to eyeball movement. The letters *A* and *B* mark subsegments whose analyses are displayed in Figs. 8 and 9

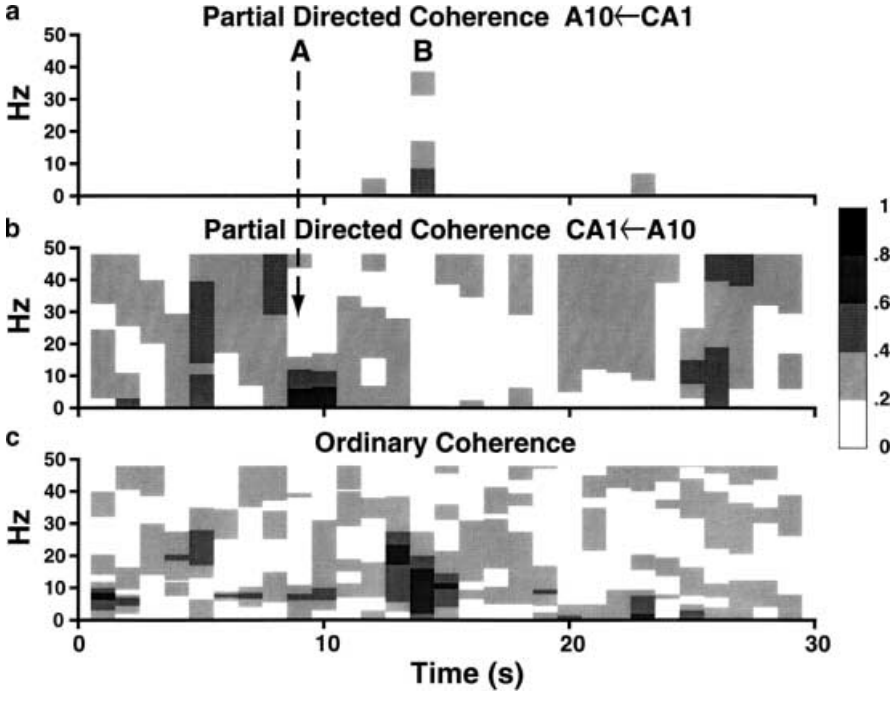

Fig. 7. **a** Gray-scale time-frequency representation of partial directed coherence (*PDC*) (computed via the simultaneous analysis of all six neuroactivity signals in Fig. 6) and ordinary coherence between *A10* and *CA1* obtained by collating estimates for adjacent 2-s-long segments (with 50% overlap): the y-axes are scaled between 0 and 48 Hz. In **a**, $|\bar{\pi}_{A10\leftarrow CA1}(f)| \cong 0$ for most of the segment; i.e., no information flows from *CA1* to *A10*, except during the spindle (*B*) when $|\bar{\pi}_{A10\leftarrow CA1}(f)| > 0$, for $0 < f < 10$ Hz, whereas in the opposite direction (**b**), $|\bar{\pi}_{CA\leftarrow A_{10}}(f)|$ enjoys continuous change along the record. During the spindle episode $|\bar{\pi}_{CA\leftarrow A}(f)| \cong 0$ leading to an observed switch in the direction of information flow between these structures. The ordinary coherence is depicted in **c**; note its higher value during the spindle event

et al. (1998), $\gamma_{ij}(f)$ represents the fraction of the power in the spectrum in $x_i(n)$ originating from each $x_j(n)$, so that it describes pairwise structure interactions that may be either direct or indirect (via the many possible pathways formed by signal propagation through intermediate structures). As such, $\gamma_{ij}(f)/DTF_{ij}(f)$ is a descriptive summary of structural interaction over all pathways linking two structures. If $\gamma_{ij}(f)/DTF_{ij}(f)$ is significant, one can at least infer the existence of indirect signal feedback. Non-null $\pi_{ij}(f)$ tell us that direct feed back is present; this reflects more closely the possible presence of active direct physical links between structures.

5.1.1 Source determination. In some cases, as in searching for signal foci (sources), one may use either $\pi_{ij}(f)$ or $DTF_{ij}(f)$. In Examples 3, 4, and 6, by working with the $\pi_{ij}(f)$ information in Figs. 2b, 3b, and 5b back into the diagrams in Figs. 2a, 3a, and 5a, respectively, would readily lead to identification of $x_1(n)$ as the focus. The same conclusion follows from $DTF_{ij}(f)$ by noting that $x_1(n)$ receives no power from the other series ($DTF_{1j}(f) = 0$ for all $j \neq 1$) while at the same time fractions of its power contribute to all $x_i(n)$ as $DTF_{i1}(f) \neq 0$. As such, previous EEG uses of $DTF_{ij}(f)$ for epileptic focus determination (Franaszczuk et al.

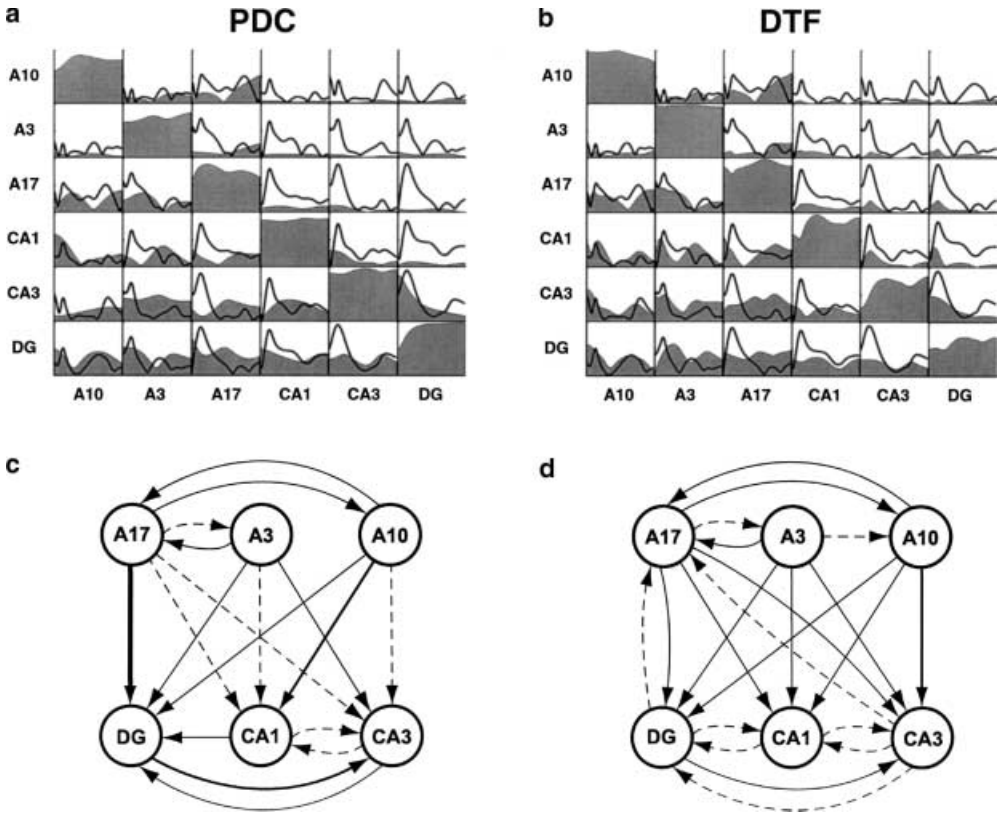

Fig. 8a–d. Pre-spindle two -second-long segment A (Fig. 6) *PDC* (**a**) and structural schematic (**c**) using Table 1 values depicting lack of hippocampal feedback to cortex. This is confirmed by *DTF* (**b**) (and its schematic, **d**). The schematics code interaction strength via arrow line type and width ($0 \leq$ no arrow $\leq 0.2 <$ dashed line ≤ 0.4 increasing width solid lines in steps of 0.2). See the text for further details

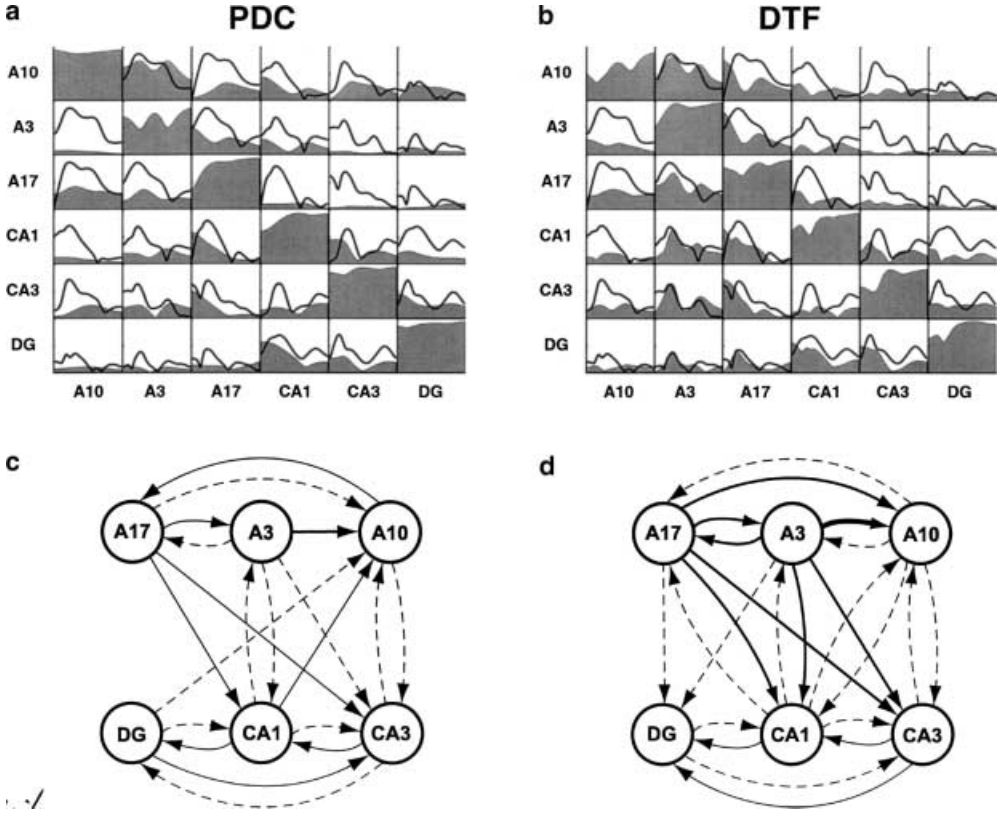

Fig. 9a–d. Spindle PDC (**a**) (Two-second-long segment B, Fig. 6) for all structures and its structural schematic (**c**) based on Table 2 values and portraying hippocampal feedback to cortex (via *CA1* to *A10*). The *DTF* (**b**) (and graph **d**) is more complex and almost fully connected, hindering clear resolution of the signal flow pattern. The schematics code interaction strength as for Fig. 8. See the text for further details

Table 1. Values of $\binom{\max|\mathrm{PDC}|}{\max|\mathrm{DTF}|}$ for the pre-spindle period (segment *A* in Fig. 6). These values were used in constructing the graphs in Fig. 8c and d. This table follows the same reading convention of source (column) to row (target) as the PDC and DTF plots

A10		$\binom{0.18}{0.25}$	$\binom{0.53}{0.58}$	$\binom{0.03}{0.06}$	$\binom{0.06}{0.10}$	$\binom{0.09}{0.09}$
CA3	$\binom{0.09}{0.13}$		$\binom{0.27}{0.28}$	$\binom{0.06}{0.14}$	$\binom{0.04}{0.12}$	$\binom{0.07}{0.17}$
A17	$\binom{0.41}{0.43}$	$\binom{0.41}{0.47}$		$\binom{0.11}{0.17}$	$\binom{0.12}{0.23}$	$\binom{0.10}{0.23}$
CA1	$\binom{0.66}{0.49}$	$\binom{0.39}{0.53}$	$\binom{0.23}{0.57}$		$\binom{0.32}{0.32}$	$\binom{0.11}{0.38}$
CA3	$\binom{0.27}{0.61}$	$\binom{0.46}{0.50}$	$\binom{0.33}{0.51}$	$\binom{0.39}{0.29}$		$\binom{0.67}{0.48}$
DG	$\binom{0.44}{0.58}$	$\binom{0.44}{0.59}$	$\binom{0.93}{0.48}$	$\binom{0.47}{0.35}$	$\binom{0.41}{0.31}$	
	A10	**A3**	**A17**	**CA1**	**CA3**	**DG**

Table 2. Values of $\binom{\max|\mathrm{PDC}|}{\max|\mathrm{DTF}|}$ for the spindle episode (segment B in Fig. 6). These values were used in constructing the graphs in Fig. 9c and d. This table follows the same reading convention of source (column) to row (target) as the PDC and DTF plots

A10		$\binom{0.77}{0.82}$	$\binom{0.32}{0.76}$	$\binom{0.49}{0.32}$	$\binom{0.33}{0.22}$	$\binom{0.31}{0.19}$
CA3	$\binom{0.09}{0.28}$		$\binom{0.49}{0.79}$	$\binom{0.32}{0.22}$	$\binom{0.06}{0.07}$	$\binom{0.14}{0.09}$
A17	$\binom{0.44}{0.37}$	$\binom{0.36}{0.68}$		$\binom{0.11}{0.34}$	$\binom{0.07}{0.18}$	$\binom{0.11}{0.13}$
CA1	$\binom{0.14}{0.20}$	$\binom{0.29}{0.65}$	$\binom{0.53}{0.66}$		$\binom{0.44}{0.41}$	$\binom{0.25}{0.28}$
CA3	$\binom{0.24}{0.27}$	$\binom{0.26}{0.65}$	$\binom{0.54}{0.72}$	$\binom{0.28}{0.22}$		$\binom{0.52}{0.28}$
DG	$\binom{0.10}{0.15}$	$\binom{0.09}{0.36}$	$\binom{0.19}{0.39}$	$\binom{0.53}{0.57}$	$\binom{0.30}{0.49}$	
	A10	**A3**	**A17**	**CA1**	**CA3**	**DG**

1994; Kaminski et al. 1997) are fully justifiable despite the larger computational complexity involved in calculations (matrix inversions are needed).

Though containing essentially the same information DC/DTF exposes it in a less clear fashion when compared to $\bar{\pi}_{ij}(f)$. When a more detailed picture is sought – as in appraising the dynamic role of anatomically separate cortical and subcortical structures – $\bar{\pi}_{ij}(f)$ is able to break up the interactions between structures into their direct pairwise components. This exposes additional details of the signal propagation between structures (Example 6).

5.2 Comments on estimation issues

In practice, PDC estimation requires the reliable fitting of MAR models, which is treated in depth elsewhere (Lutkepöhl 1993). This is also true for DC/DTF. On a whole the subject of fitting MAR models is not without its subtleties, such as model order estimates (choice of p in Eq. 12), diagnostic tests on model residues, and perhaps most importantly the issue of joint time series stationarity whereupon the estimation of $a_{ij}(r)$ is based (see Bernasconi and König 1999). One important point is that the issue of stationarity may be approached in the physiological setting by an empirical appraisal of the behavioral state of the animal under observation. Another important limitation that affects both DC and PDC is the adequacy of modelling neural signals linearly, as in some contexts nonlinear interaction models may be more appropriate.

Reliable structural inference depends heavily on the issue of statistical significance (rejecting interaction absence) via PDC (and/or DTF). Determination of rigorous estimate significance – even asymptotic – remains an important and largely open problem for these estimators. Preliminary simulation studies indicate that statistical significance depends not only on signal length but also on N, the number of simultaneously processed structures. In practical applications, averaging results from similar physiological scenarios was used in examples of DTF analysis by Kaminski et al. (1997). Similar procedures can be used with PDC estimation.

Remark 6. To our knowledge, the only published results on significance are due to Schnider et al. (1989), who have made extensive simulations of DC for $N = 2$ leading to a choice of a 0.05 threshold above which interaction is deemed significant.

5.3 Conclusions and final remarks

This paper draws the connection between Granger causality as the basis for prior structural descriptors such as DC/DTF and the new one represented by PDCF/PDC, and their relationships as terms in decom-

positions of ordinary and partial coherences respectively. While PDC portrays the relative strength of direct pairwise structure interactions, DC/DTF represents a balance of signal power that spreads from one structure to another over many possible alternative pathways.

With the help of signal preprocessing via adequate kernels (Baccalá and Sameshima 1998), the PDC technique can be applied to the simultaneous analysis of single and multi-unit activity from many electrodes. Examples of PDC in this kind of analysis appeared recently in Sameshima and Baccalá (1999).

Acknowledgements. This research was funded by FAPESP grant 99/07641-2 to L.A.B. FAPESP grant 96/12118-9 to K.S. and PRONEX grant 41.96.0925.00 to K.S. and L.A.B.

References

Baccalá LA, Sameshima K (1998) Directed Coherence: a tool for exploring functional interactions among brain structures. In: Nicolelis MAL (ed) Methods for neural ensemble recordings. CRC Boca Raton, Fla., pp 179–192

Baccalá LA, Sameshima K, Ballester G, Valle AC, Timo-Iaria C (1998) Studying the interaction between brain structures via directed coherence and Granger causality. Appl Signal Process 5: 40–48

Barlow JS (1979) Computerized clinical electroencephalography in perspective. IEEE Trans Biomed Eng 26: 377–391

Bendat JS, Piersol AG (1986) Random data: analysis and measurement procedures, 2nd edn. John Wiley, New York

Bernasconi C, König P (1999) On the directionality of cortical interactions studied by structural analysis of electrophysiological recordings. Biol Cybern 81: 199–210

Bressler SL, Coppola R, Nakamura R (1993) Episodic multiregional cortical coherence at multiple frequencies during visual task performance. Nature 366: 153–156

Duckrow RB, Spencer SS (1992) Regional coherence and the transfer of ictal activity during seizure onset in the medial temporal lobe. Electroencephalogr Clin Neurophysiol 82: 415–422

Eggermont JJ (1990) The correlative brain: theory and experiment in neural interaction. Springer, Berlin Heidelberg New York

Franaszczuk PJ, Blinowska KJ, Kowalczyk M (1985) The application of parametric multichannel spectral estimates in the study of electrical brain activity. Biol Cybern 51: 239–247

Franaszczuk PJ, Bergey GK, Kaminski MJ (1994) Analysis of mesial temporal seizure onset and propagation using the directed transfer function method. Electroencephalogr Clin Neurophysiol 91: 413–427

Gevers MR, Anderson BDO (1981) Representation of jointly stationary stochastic feedback processes. Int J Control 33: 777–809

Gevers MR, Anderson BDO (1982) On jointly stationary feedback-free stochastic processes. IEEE Trans Autom Control 27: 431–436

Geweke J (1982) Measurement of linear dependence and feedback between multiple time series. J Am Stat Assoc 77: 304–313

Granger CWJ (1969) Investigating causal relations by econometric models and cross-spectral methods. Econometrica 37: 424–438

Kaminski MJ, Blinowska KJ (1991) A new method of the description of the information flow in the brain structures. Biol Cybern 65: 203–210

Kaminski MJ, Blinowska KJ, Szelenberger W (1997) Topographic analysis of coherence and propagation of EEG activity during sleep and wakefulness. Electroencephalogr Clin Neurophysiol 102: 216–227

Kocsis B, Thinschmidt JS, Kinney GG, Vertes RP (1994) Separation of hippocampal theta dipoles by partial coherence analysis in the rat. Brain Res 660: 341–345

Korzeniewska A, Kasicki S, Kaminski MJ, Blinowska KJ (1997) Information flow between hippocampus and related structures during various types of rat's behavior. J Neurosci Methods 73: 49–60

Lopes da Silva FH, Van Lierop THMP, Schrijer CF, Van Leewen WS (1973) Organization of thalamic and cortical alpha rhythms: spectra and coherence. Electroencephalogr Clin Neurophysiol 35: 627–639

Lutkepöhl H (1993) Introduction to multiple time series analysis, 2nd edn. Springer, Berlin Heidelberg New York

Melssen WJ, Epping WJM (1987) Detection and estimation of neural connectivity based on cross correlation. Biol Cybern 57: 403–414

Pawelzik K (1994) Detecting coherence in neuronal data. In: Domany E, Hemmen JLV, Schulten K (eds) Models of neural network II. Springer, Berlin Heidelberg New York, pp 253–286

Saito Y, Harashima H (1981) Tracking of information within multichannel EEG record – causal analysis in EEG. In: Yamaguchi N, Fujisawa K (eds) Recent advances in EEG and EMG Data Processing. Elsevier, Amsterdam, pp 133–146

Sameshima K, Baccalá LA (1999) Using partial directed coherence to describe neuronal ensemble interactions. J Neurosci Methods 94: 93–103

Schnider SM, Kwong RH, Lenz FA, Kwan HC (1989) Detection of feedback in the central nervous system using system identification techniques. Biol Cybern 60: 203–212

Toyama K, Kimura H, Tanaka K (1981) Cross-correlation analysis of interneuronal connectivity in cat visual cortex. J Neurophysiol 46: 191–201